AIAA JOURNAL
Vol. 40, No. 10, October 2002

Numerical Simulation of Unsteady Turbulent Flow Around Maneuvering Prolate Spheroid

Shin Hyung Rhee* and Takanori Hino†
National Maritime Research Institute, Tokyo 181-0004, Japan

A three-dimensional Reynolds averaged Navier–Stokes method for unsteady turbulent flow around a maneuvering vehicle was developed and applied to a model problem concerning an extreme case of submarine maneuvers. A body force term is added in the momentum equations to take into account the inertial motion in the body-fixed coordinate system. The Spalart and Allmaras turbulence model is employed for turbulence closure. An artificial compressibility is introduced into the continuity equation for velocity–pressure coupling. The governing equations are discretized by second-order accurate finite volume method in space and second-order accurate backward scheme in time. The computational results are analyzed with global and local quantities and validated by comparison with experimental data. Overall, the present method performs quite well in predicting the unsteady flow phenomena associated with a maneuvering prolate spheroid, and the results compare well with available experimental data. Comparisons of steady and unsteady flow results show lags in the flowfield development and delays of flow separation in unsteady flow cases, indicating that unsteady flow phenomena cannot be well understood by simple extensions of steady or quasi-steady computational results. Comparisons with experimental data reveal that the isotropic eddy viscosity turbulence model used does not adequately resolve the vortical flow in separated regions.

I. Introduction

THE computational fluid dynamics (CFD) techniques for vehicle hydrodynamics have shown substantial advancement over the last two decades and are being increasingly used in design processes. Applications for off-design and unsteady flows are, however, still relatively rare. To expand the dynamic performance of vehicles such as submarines and aircraft beyond conventional regimes, it is of crucial importance to study truly unsteady, high-excursion, high-Reynolds-number flows. Experimental studies (e.g., Wetzel and Simpson[1]) have shed light on the significance of the unsteady flow evolution and the distinction between steady and unsteady flows; however, it is expensive and quite complicated to conduct experiments that meet certain conditions required for mentioned flow regimes. CFD approaches also have been attempted for maneuvering vehicles (e.g., Taylor et al.[2]); however, detailed observation and analysis of the flowfield and rigorous validation have not been provided. As the demand for CFD techniques in simulations of various real-world situations increases, more sophisticated CFD codes, which are capable of dealing with not only the complex flowfield around a body but also vehicle dynamic performance, must be developed.

The present study concerns the development of a CFD code and assessment of its capability through application to maneuvering problems, which require a considerable amount of study to meet various rules and regulations for safety and effective performance. The objectives of the present study are threefold: first, development of a three-dimensional unsteady Reynolds averaged Navier–Stokes (RANS) method for maneuvering problems; second, application of the method to a model problem, which can be described as an extreme case of submarine maneuvers; and third, provision of guidelines for future code development and implementation in concurrent engineering design procedures.

Received 30 November 2001; revision received 4 March 2002; accepted for publication 6 April 2002.

*Science and Technology Agency Fellow, Ship Performance Division; currently Computational Fluid Dynamics Engineer, Aerospace Industry Team, Fluent, Inc., Lebanon, NH 03766.

†Chief, Computational Fluid Dynamics Section; hino@nmri.go.jp.

The paper is organized as follows. Section II provides a review of relevant studies. Section III contains a description of the model problem and mathematical formulation used for the present unsteady RANS method. In Sec. IV, the numerical method employed is described. Section V presents the uncertainty assessment results, simulation results, comparison with experimental data, and analysis of the flowfield with regard to unsteady separated flow physics. Section VI contains concluding remarks and recommendations for future code development.

II. Relevant Work

Studies of three-dimensional separated flows, which are a prerequisite for understanding the flowfield around a maneuvering vehicle, have been carried out by flow visualization,[3,4] theoretical analysis based on flow topology,[5] and numerical simulation.[6–8] Despite the limitations of rather small incidence angles and low Reynolds numbers, these studies helped understand the physics of how three-dimensional boundary layer evolves as it gradually shears into a vortex rollup and then into streamwise vortices. Especially, types of three-dimensional separation and development of open separation proposed by Wang[6] have been widely adopted in numerous studies and have served as a base of interpretation of computational results.

Based on the knowledge obtained through studies of three-dimensional separated flows and in response to the need in aero- and hydrodynamic design community, the flowfield measurements around an inclined body have been conducted using various experimental techniques. The measurements of mean velocity, pressure, and shear stress of a 6:1 prolate spheroid with incidence angles of 10 and 30 deg were made in the monumental experiments by Meier et al.[9,10] For the same geometry, Barber and Simpson[11] reported mean velocity and turbulence, which was extended further by Chesnakas and Simpson.[12] They developed miniature laser Doppler velocimetry and made simultaneous measurements of velocity and pressure, to provide plots of mean velocity, skin friction, mean and fluctuating pressure, and turbulence kinetic energy. Their plots of turbulence anisotropy show that there is little correlation between the flow gradient and the turbulent shear stress angles over large regions of the flow. The anisotropic turbulence in the separated region is also evident by the reduced eddy viscosity and mixing length[13] and the increasing difference in direction between the velocity gradient and the shear stress vector.[14]

Along with experimental studies, a number of RANS simulation results of the flowfield around an inclined body have been reported

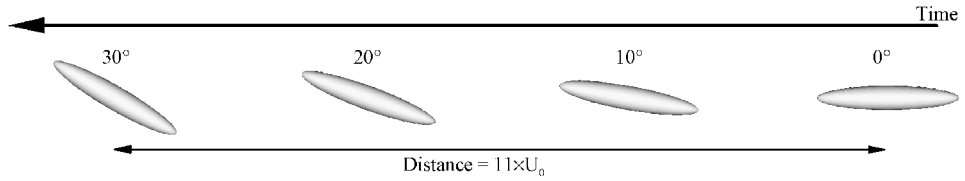

Fig. 1 Schematic of the pitch-up maneuver of a prolate spheroid.

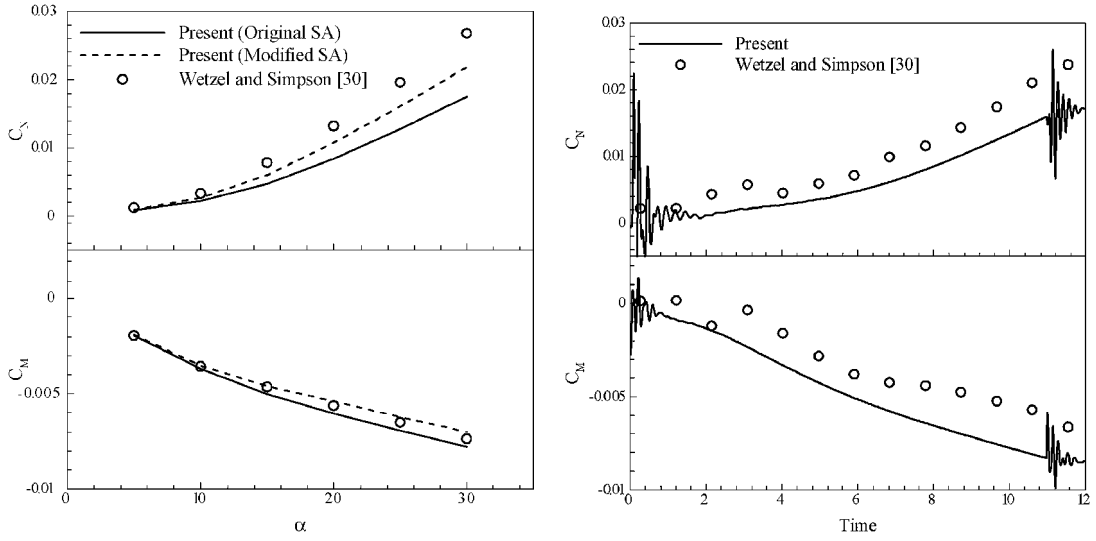

Steady case **Unsteady case**

Fig. 2 Normal force and pitch moment.

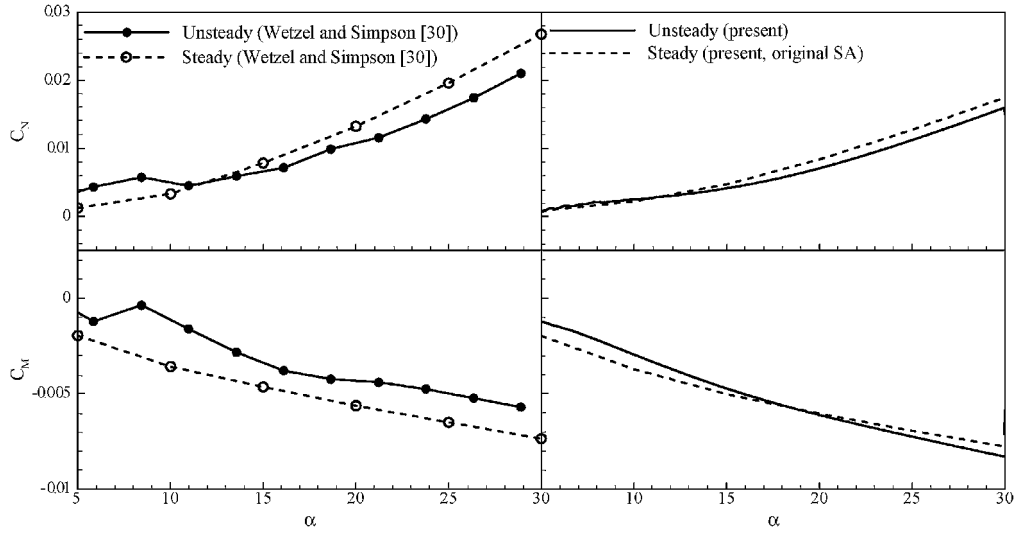

Fig. 3 Difference of normal force and pitch moment between steady and unsteady cases.

in the past decade.[15–22] All of them show quite good performance in predicting the global, for example, forces and moments, and local, for example, mean velocity and pressure, quantities. However, it has been recognized that isotropic eddy viscosity turbulence models do not adequately resolve the vortical flow in separated regions. This is attributed to the general tendency of overpredicted eddy viscosity in separated regions and underlying assumption of the turbulence isotropy.

Unsteady flows around bodies undergoing time-dependent maneuvers have been studied, generally, using experimental techniques. Most studies focused on slender axisymmetric bodies, such as an ogive cylinder[23,24] and hemisphere-/conical-nose cylinder,[25–27] to apply the findings to missile aerodynamics. Researchers at Virginia Polytechnic Institute and State University extended their views and conducted experiments for a 6:1 prolate spheroid, with applications to underwater vehicles undergoing maneuvering motions in mind. They reported detailed measurement data and analyses of unsteady crossflow separation.[1,28–30] They also found that significant lags occur in the flowfield and that separation is delayed at all locations during the maneuvers compared to the steady cases. One of their conclusions was, therefore, that the lags in the development of the flowfield can lead to different flow topologies for an unsteady case, suggesting the necessity of a different approach for studies of unsteady flows with time-dependent maneuvers.

Recently, an increasing number of studies using CFD approaches to maneuvering problems have been reported: Sung et al.[31] presented simulations of axisymmetric bodies in steady turning; Sato et al.[32] presented results of Z maneuvering tests for two tanker hull forms; Stanek and Visbal[33] and Taylor et al.[2] presented results for cases with

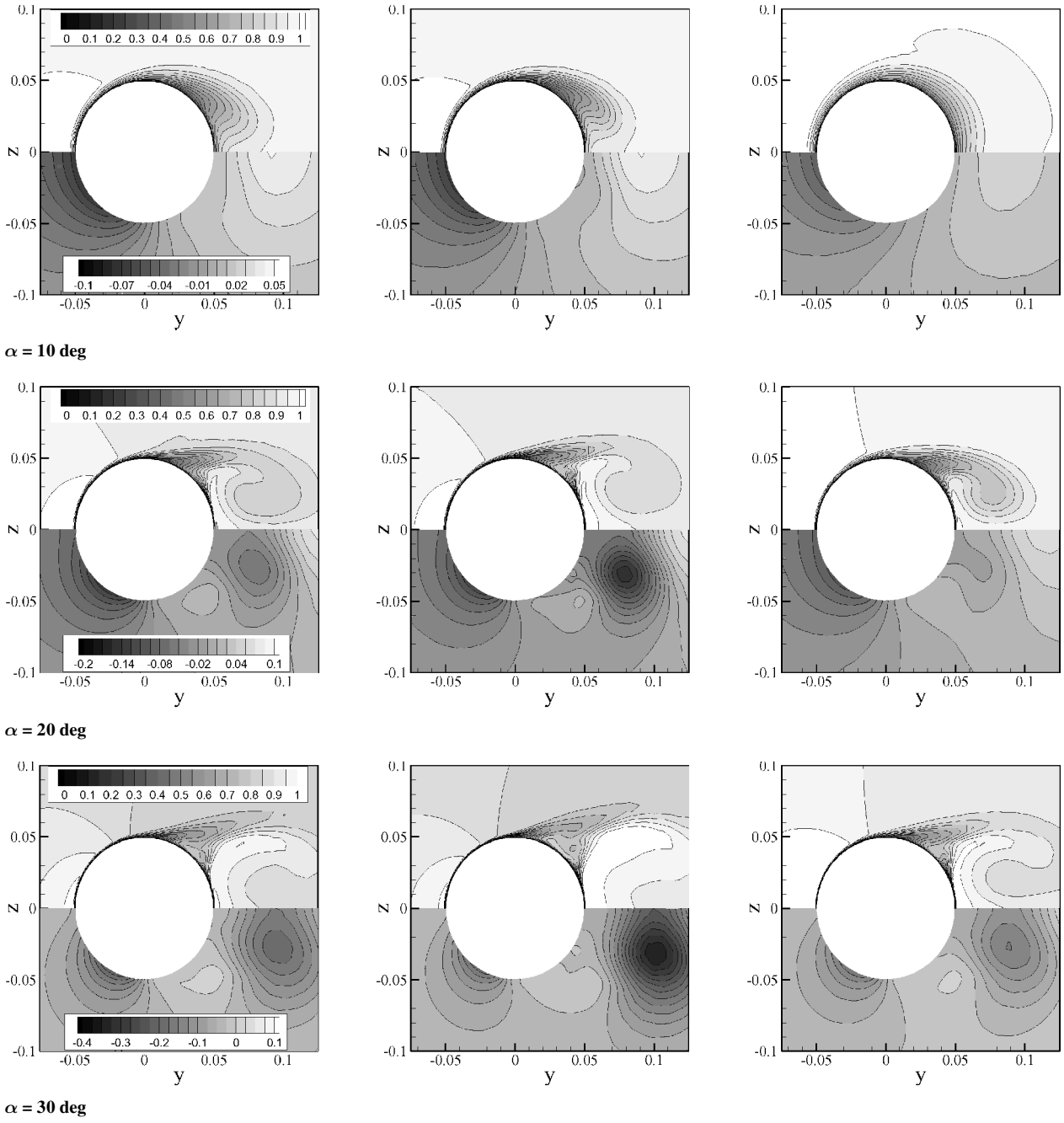

Fig. 4 Contours of U (upper half) and p (lower half) on crossplane at $x = 0.9$: steady with original SA (left), steady with modified SA (center), and unsteady (right).

more severe maneuvering motions, such as pitching, plunging, and turning; and McDonald and Whitfield[34] presented results for self-propelled maneuvering underwater vehicles. In these studies, RANS equations were solved with eddy viscosity turbulence models, and a body force term that expresses body motions is included in the governing equations, except for Stanek and Visbal.[33] These studies show quite promising results; however, conditions are limited, and detailed analysis and rigorous validation are not presented, such that considerably more work is needed.

III. Model Problem and Mathematical Formulation

The model problem of the present study is turbulent flow around a 6:1 prolate spheroid in a pitch-up maneuver. The pitch-up maneuver is a simple linear ramp from 0 to 30 deg in 11 nondimensional time units, $t =$ time (L/U_0), where U_0 is freestream velocity and L is the spheroid length. It resembles the submarine maneuver[1] that was modeled after data for a full-scale submarine during the initial transient portion of a turning maneuver and is suitable for the objectives of the present study. The spheroid is pitched about its center, which is consistent with the experimental setup.[1] Figure 1 shows the schematic of the pitch-up maneuver. Computational conditions are set following the experimental conditions, except for the sting at the rear of the model, wind-tunnel walls, and the slight backward motion of the model caused by limitations of plunge–pitch motion coordination in the experimental facility. Turbulent flow is considered, where Reynolds number $Re = U_0 L/\nu$, defined in terms of U_0, L, and kinematic viscosity ν, is 4.2×10^6. Experimental data from Hoang et al.,[29] Wetzel,[‡] and Wetzel and Simpson[30] are used for comparison.

The mathematical equations for the present study are written in the Cartesian coordinate system fixed to the body. Therefore, the inertia forces due to coordinate system transformation, that is, from the space fixed $\boldsymbol{x}_g = (x_g, y_g, z_g)$ to the body fixed $\boldsymbol{x} = (x, y, z)$, which

[‡]Data available online at http://www.aoe.vt.edu/aoe/physical/dyppir/dyp_diss.htm [cited 1 March 2000].

are nondimensionalized by L, should be added as a body force term. When vector notation is used, the inertia forces due to the transformation are

$$\boldsymbol{b} = -2\boldsymbol{\Omega} \times \boldsymbol{U} - \boldsymbol{\Omega} \times (\boldsymbol{\Omega} \times \boldsymbol{r}) - \frac{\partial \boldsymbol{\Omega}}{\partial t} \times \boldsymbol{r} - \frac{\partial \boldsymbol{V}_s}{\partial t} \tag{1}$$

where $\boldsymbol{\Omega}$ and $\boldsymbol{V}_s$ are the angular and translation velocity vectors of the body-fixed coordinate system, respectively, and $\boldsymbol{U} = [U \quad V \quad W]^T$ and $\boldsymbol{r}$ are flow velocity normalized by U_0 and position vectors in the body-fixed coordinate system, respectively. For the present study, $\boldsymbol{\Omega}$ is normalized by U_0/L and retains only one component, that is,

$$\left[0 \quad 0 \quad \frac{\partial \alpha}{\partial t}(= 0.0476)\right]^T$$

where α is the pitch angle in radians.

The governing equations are continuity and unsteady three-dimensional RANS equations for incompressible flow, written as

$$\nabla \cdot \boldsymbol{U} = 0 \tag{2}$$

$$\frac{\mathrm{D}\boldsymbol{U}}{\mathrm{D}t} + \nabla p - \nabla \cdot \boldsymbol{\tau} + \boldsymbol{b} = 0 \tag{3}$$

where p is pressure normalized by ρU_0^2, $\boldsymbol{\tau}$ is the shear stress tensor, and $\boldsymbol{b} = [b_x \quad b_y \quad b_z]^T$ is the body force term described earlier.

The one-equation turbulence model by Spalart and Allmaras[35] (SA) is employed for the present study, which solves a transport equation for eddy viscosity. A modified version proposed by Dacles-Mariani et al.[36] is also implemented for steady flows to evaluate the influence of turbulence prediction on the overall solution behavior. The modification contains a new evaluation method for the vorticity in the eddy viscosity production term, such that the $|\boldsymbol{\omega}|$ is replaced by $|\boldsymbol{\omega}| + C_v \min(0, |\boldsymbol{S}| - |\boldsymbol{\omega}|)$, where C_v is an arbitrary constant and $|\boldsymbol{S}|$ is the strain rate magnitude, to reduce the eddy viscosity in the regions where $|\boldsymbol{\omega}|$ exceeds $|\boldsymbol{S}|$, for example, in the vortex core. The value of C_v (= 20) is based on a parametric study with the steady flow at $\alpha = 20$ deg. When C_v is set to the original value (= 4) proposed by Dacles-Mariani et al.,[37] the eddy viscosity is overpredicted and vortices are suppressed. When C_v is set to 10 times the original value (= 40), the flowfield shows a limiting cycle behavior and oscillatory solutions are obtained.

The solution domain resembles a half of an egg with extent $-2.0 \le x \le 4.0$, $-2.0 \le y \le 2.0$, $0 \le z \le 2.0$, and the origin at the

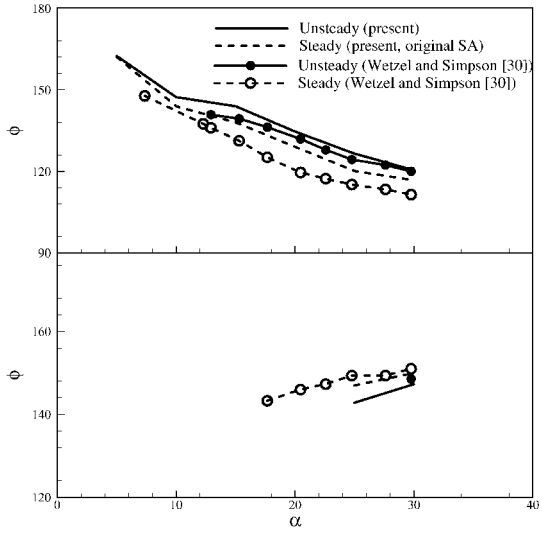

Fig. 5 Separation locations: primary separation (top) and secondary separation (bottom).

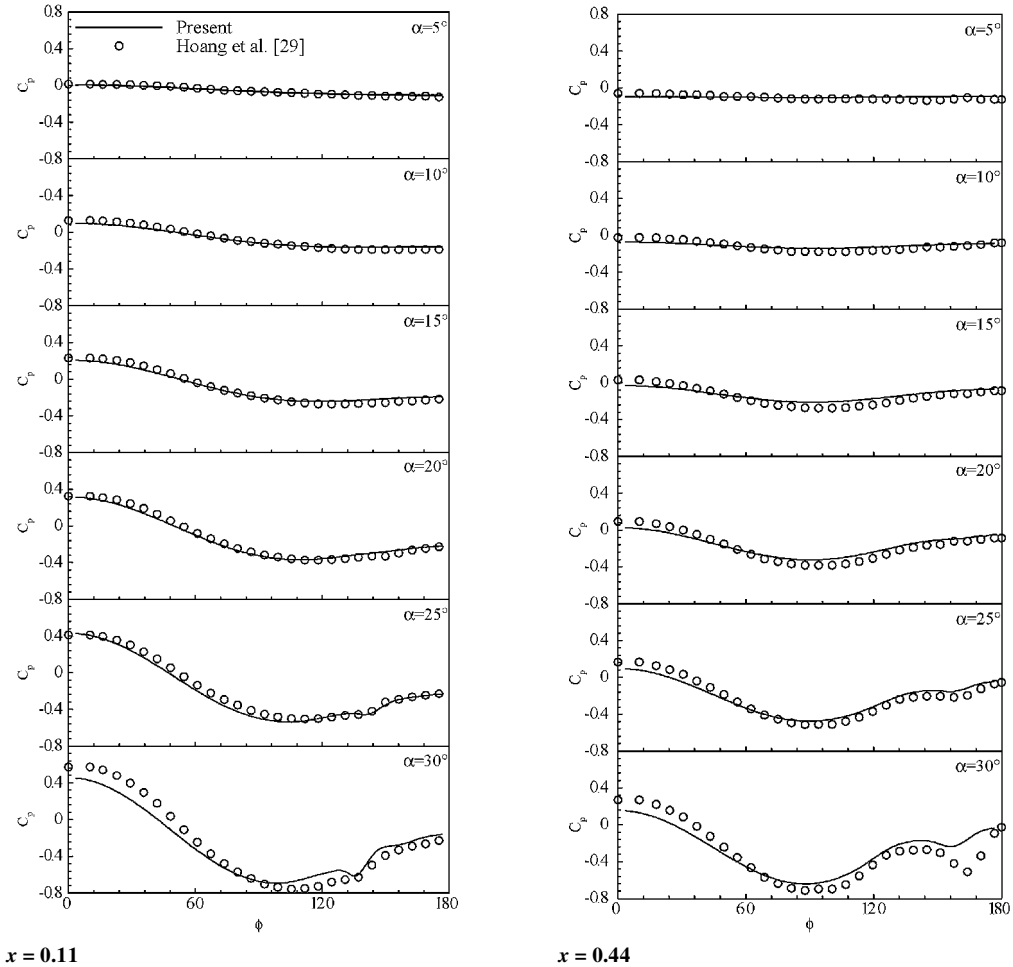

***x* = 0.11** ***x* = 0.44**

Fig. 6 Pressure coefficient at various axial locations.

body center. Both the asymmetry in the flow and wind-tunnel blockage effects were negligible in the experimental studies[29,30] (also Wetzel[‡]), and this justifies the present domain configuration. The boundary condition on each boundary is as follows: 1) On the body, the no-slip condition with $\partial p/\partial n = 0$ (steady flow) or $\partial p/\partial n = b_n$ is imposed, where b_n is the face-normal component of the body force (unsteady flow). 2) On the outer boundary up to $x = -0.5$, $\boldsymbol{U}(\boldsymbol{r}_g) = -\boldsymbol{V}_s$ (steady flow) or $\boldsymbol{U}(\boldsymbol{r}_g) = -\boldsymbol{V}_s - \boldsymbol{\Omega} \times \boldsymbol{r}_g$ (unsteady flow) is imposed, where $\boldsymbol{r}_g$ is the position vector in the space-fixed coordinate system, with zero-gradient pressure and freestream eddy viscosity of $0.01/Re$. 3) On the remaining outer boundary, zero-gradient perturbation velocity, that is, $\partial \boldsymbol{U}(\boldsymbol{r}_g)/\partial n = 0$ (steady flow) or $\partial[\boldsymbol{U}(\boldsymbol{r}_g) + \boldsymbol{\Omega} \times \boldsymbol{r}_g]/\partial n = 0$ (unsteady flow) is imposed, with $p = 0$ and zero-gradient eddy viscosity. 4) On the symmetry plane, $\partial(U, V, p, \nu_t)/\partial n = W = 0$ is imposed. The initial condition for unsteady flow calculations is a corresponding steady flow solution at $\alpha = 0$ deg.

IV. Numerical Method

A numerical method was developed and implemented in a computer code for the solution of the unsteady RANS mathematical formulation and modeling described in the preceding section. The main flow solver was developed by Hino,[37] and a variety of validation cases including free-surface flows around practical ship hull forms were carried out.[38,39] The code's capabilities were extended to unsteady flow computations following Rogers et al.,[40] and results of fundamental test cases were reported by Rhee and Hino.[41] Also detailed results of three-dimensional steady turbulent flow separation around a prolate spheroid with modified SA model are available by Rhee and Hino.[22] In the present study, the unsteady flow computation procedures are refined, and a body force term and boundary conditions for general maneuvering motions are included.

An artificial compressibility is introduced into the continuity equations to couple a pressure field with the corresponding velocity one. The finite volume method (FVM) is adopted for spatial discretization. The computational domain is meshed into unstructured polyhedral cells. Flow variables are stored at the center of each cell. For inviscid fluxes, the second-order accurate upwind scheme based on the flux-difference splitting of Roe[42] with the MUSCL approach is employed. Viscous fluxes are evaluated by the second-order accurate central scheme.

After the spatial discretization, time-derivative terms are discretized using Euler backward and second-order accurate backward scheme for pseudo- and physical time-derivative terms, respectively. Note that the physical time-derivative term is required for unsteady flow calculations only. The local time stepping is employed for the pseudo-time increment, so that the Courant–Friedrichs–Lewy number based on it is globally constant.

The resulting linear equation is solved by the symmetric Gauss–Seidel iteration. The pseudo-time iteration continues until the averaged pressure residual between two consecutive pseudo-time iterations, that is, continuity equation imbalance, reaches a convergence criterion, which is three orders of magnitude drop, or the iteration number reaches its preset maximum, which is between 10 and 50 in the present study. Because of the abrupt start and stop at the beginning and end of the pitch-up maneuver, special care should be taken in the evaluation of the body force term: Only half of the body force is taken into account at the moments when the maneuver starts and stops, that is, central differencing over a time span of one time step before and after the moment is used.

To exploit the simplicity of the geometry and also to maximize the numerical accuracy and efficiency, hexahedral cell grids were

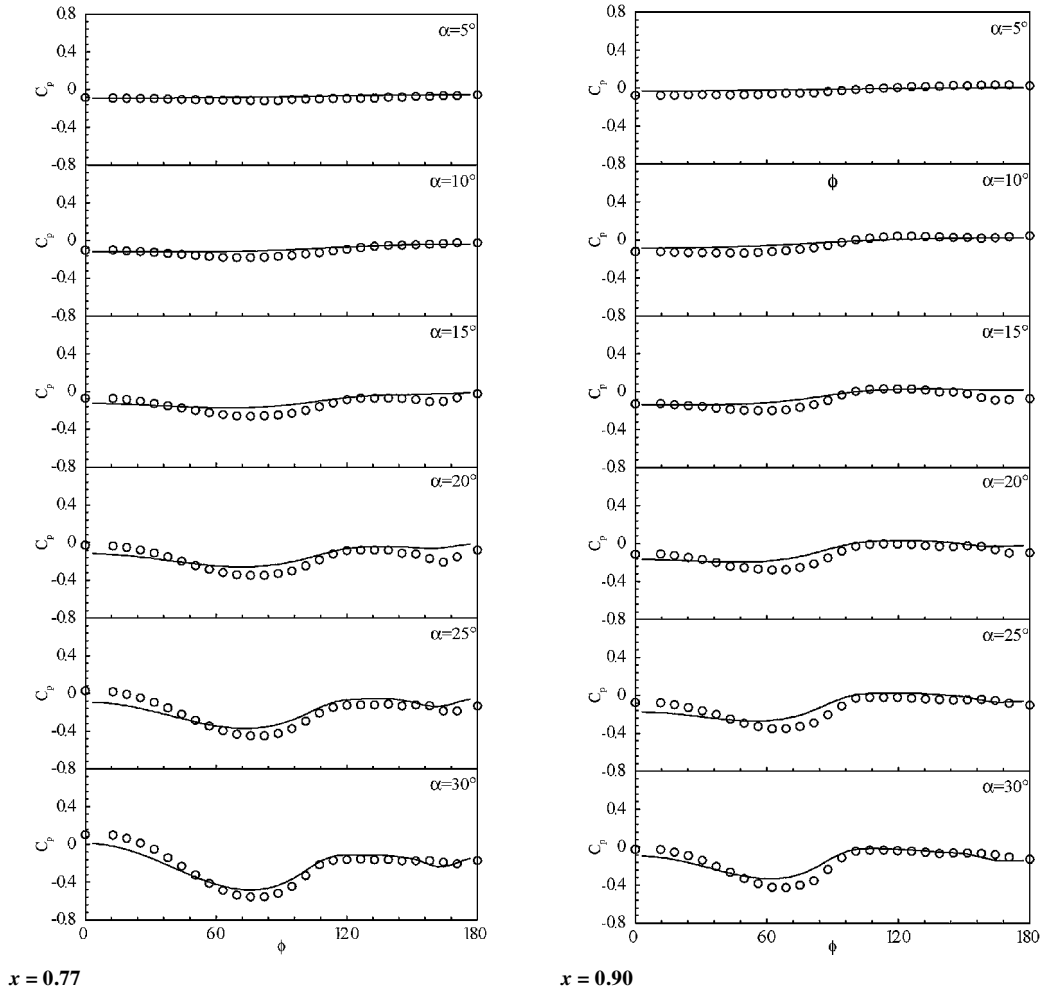

***x* = 0.77** ***x* = 0.90**

Fig. 6 Pressure coefficient at various axial locations (continued).

generated using GRIDGEN™ software by mixed algebraic/elliptic method. The average minimum spacing in the normal direction is about 1×10^{-5}.

V. Results and Comparison Data

The simulation results are analyzed here using the global force and moment, separated flowfield observation, separation location, and pressure and skin-friction coefficients. Uncertainty analysis was carried out for the pitch-up maneuver case, and the results are presented in this section. Comparisons are made with the available experimental data, and the difference of features between the steady and unsteady flows is discussed with regard to an extension of steady flow results to analysis of unsteady flows. Note that the unsteady flow computations were done using the original SA model only, and all of the presentation in this section is made with the original SA model results, unless explicitly mentioned.

To evaluate the numerical uncertainties associated with the present results, the concept of a grid convergence index proposed by Roache[43] is adopted. Three parameters, that is, grid size, time-step size, and pseudo-time iteration number, with three different levels, that is, fine, medium, and coarse, are considered for normal force coefficient, $C_N =$ normal force$/\frac{1}{2}\rho U_0^2 L^2$ at $t = 5.5$, that is, the halfway point of the pitch-up maneuver. C_N is normal to the flow direction and believed to be a global quantity that is sensitive to the parameters selected. Local quantities were not considered for uncertainty analysis and more rigorous assessment is recommended for future work. The order of accuracy,

$$p = \frac{\ell n[(\varphi_{\text{medium}} - \varphi_{\text{coarse}})/(\varphi_{\text{fine}} - \varphi_{\text{medium}})]}{\ell n(r)}$$

where φ_{coarse}, φ_{medium}, and φ_{fine} are solutions at coarse, medium, and fine levels, respectively, and r is refinement ratio, is presented in Table 1, along with the Richardson extrapolated value,

$$RE = \varphi_{\text{fine}} + \frac{\varphi_{\text{fine}} - \varphi_{\text{medium}}}{r^p - 1}$$

and convergence index (CI),

$$\text{CI} = |\varepsilon|/(r^p - 1)$$

where

$$|\varepsilon| = \left| \frac{\varphi_{\text{medium}} - \varphi_{\text{fine}}}{\varphi_{\text{fine}}} \right|$$

The value of r for grids is obtained by the effective grid refinement ratio,[43] $(N_{\text{fine}}/N_{\text{medium}})^{1/D} = (N_{\text{medium}}/N_{\text{coarse}})^{1/D} = 1.59$, where N is number of cells and D is the dimension of the problem. On the other hand, the average values of refinement ratio, that is, $r = (r_{\text{fine-medium}} + r_{\text{medium-coarse}})/2 = 2.25$, are used for convergence studies with time-step size and pseudo-time iteration number. Based

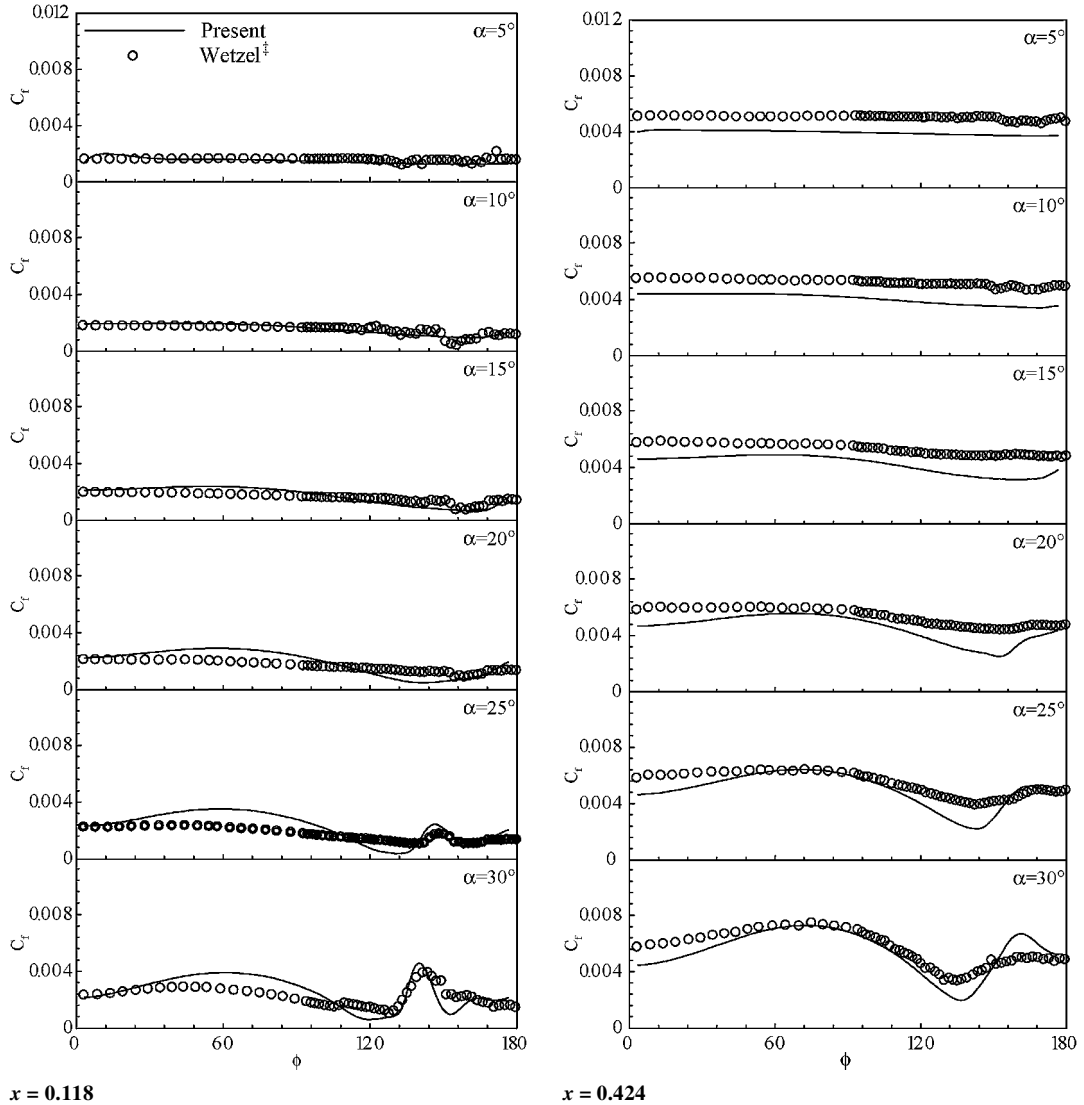

***x* = 0.118** ***x* = 0.424**

Fig. 7 Skin-friction coefficient at various axial locations.

on these convergence studies, which show less than 4.7% of uncertainties from the corresponding Richardson extrapolated values, and considering the current available computational resources, results with the fine grid (345,600 cells), medium time-step size (0.01), and medium pseudo-time iteration number (25) are presented and compared with the experimental data in the following.

The normal force C_N and pitch moment C_M = pitch moment/$\frac{1}{2}\rho U_0^2 L^3$ coefficients are selected for force and moment analysis because they are the most important global quantities in maneuvering motions. Figure 2 shows C_N and C_M for steady and unsteady flows with experimental data.[30] In both cases, the errors, which are defined as the difference between experimental data and computational results, in C_N and C_M increase up to 38.2% with increasing α, or equivalently time, which implies the difficulty of simulating strongly separated flows accurately at large pitch angles. The errors in steady flow are reduced by applying the modified SA model, which suggests a large dependency of simulation results on the turbulence modeling. The abrupt start and stop of the pitch-up maneuver cause large oscillations at the beginning and end of the maneuver in both experimental and computational results, although experimental data are shown at several points only for clarity.

Table 1 Numerical uncertainty assessment

Parameter	C_N	ε	CI	p
	Grid			
Coarse (21,600 cells)	4.67×10^{-3}	——	——	1.495
Medium (86,400 cells)	4.33×10^{-3}	7.85×10^{-2}	7.85×10^{-2}	——
Fine (345,600 cells)	4.16×10^{-3}	4.69×10^{-2}	4.69×10^{-2}	——
Richardson extrapolated value	3.99×10^{-3}	——	——	——
	Time-step size			
Coarse (0.025)	4.72×10^{-3}	——	——	2.485
Medium (0.01)	4.16×10^{-3}	1.35×10^{-1}	2.07×10^{-2}	——
Fine (0.005)	4.08×10^{-3}	2.46×10^{-2}	3.79×10^{-3}	——
Richardson extrapolated value	4.04×10^{-3}	——	——	——
	Pseudo-time iteration number			
Coarse (10)	4.64×10^{-3}	——	——	4.719
Medium (25)	4.16×10^{-3}	1.19×10^{-1}	2.65×10^{-3}	——
Fine (50)	4.04×10^{-3}	2.67×10^{-2}	5.93×10^{-4}	——
Richardson extrapolated value	4.04×10^{-3}	——	——	——

Figure 3 presents the difference of trends in C_N and C_M between steady and unsteady flows. The overall trend is consistent with the experimental one, that is, larger unsteady flow C_N and C_M after the beginning of the maneuver and smaller near the end, except for C_M in the final stage of the maneuver. The smaller C_N and C_M in the latter part of the maneuver indicate delays in separation, which corresponds to higher pressure in the leeward side of the body.

The influence of turbulence modeling on the velocity and pressure fields is displayed by the contours of U and p on the crossplane at $x = 0.9$ in Fig. 4. For steady flow at $\alpha = 10$ deg, the influence is small, although the use of modified SA model yields slightly stronger separation in U contours. For steady flow at $\alpha = 20$ deg, however, the influence of the use of the modified SA model is obvious as clearly indicated by the existence of lower leeward side pressure. This suggests that the modified SA model can improve the prediction of highly vortical flows through suppression

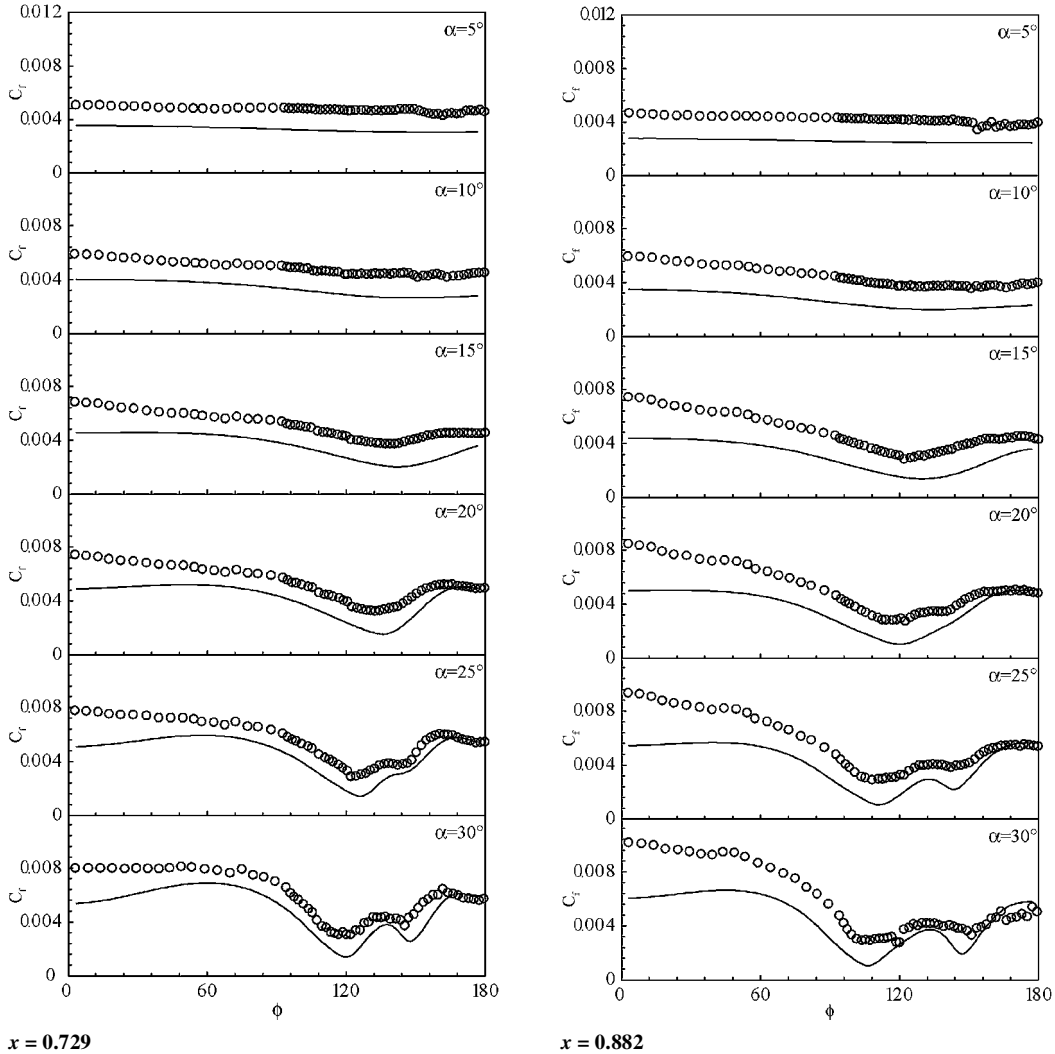

***x* = 0.729** ***x* = 0.882**

Fig. 7 Skin-friction coefficient at various axial locations (continued).

of eddy viscosity production in the region where the magnitude of vorticity exceeds that of the strain rate, such as in the vortex core.

Figure 4 also shows the delayed separation and smaller extent vortices during the pitch-up maneuver. The delayed separation will be discussed later along with separation locations. The difference in leeward side pressure between steady and unsteady flow cases accounts for the difference in C_N and C_M at the same incidence angles, that is, higher leeward side pressure can be related to lower C_N and C_M, and vice versa, as shown in Fig. 3.

Figure 5 presents primary and secondary separation locations vs α at $x = 0.729$. Note that, in the presentation hereafter, ϕ is 0 deg at the symmetry plane on the windward side and 180 deg on the leeward side. The minima in the wall shear are taken as separation locations following Wetzel and Simpson.[1] Experimental data[30] are also presented for comparison. Accurate prediction of surface pressure gradient, for which the overall turbulent flow should be well resolved, leads to accurate prediction of strength and direction of crossflow. Separation location and the strength and extent of detached vortices are closely tied with this crossflow around the body. The computational results show slightly delayed separation formations, and this can be attributed to the eddy viscosity overprediction with SA model, that is, stronger fluctuation and mixing help the flow stay attached. The windward and leeward side shifts of primary and secondary separation locations, respectively, are, however, well predicted. The strong crossflow driven by large pressure gradient in the circumferential direction at large α accounts for the former, whereas stronger primary separation and the resulting vortex account for the latter. The trend in the lag of separation location and small secondary separation during the pitch-up maneuver is also properly captured. The separations are delayed in the pitch-up maneuver case due to the history effect, which is an effect dependent on the true total path the particle has traversed.[1]

Pressure coefficients, $C_p = p/\frac{1}{2}\rho U_0^2$, at various axial locations, $x = 0.11, 0.44, 0.77$, and 0.90, are presented in Fig. 6 for increasing pitch angles. The experimental data[29] are also shown for comparison. The overall agreement between the computational and the experimental results is quite good, and the flow development during the pitch-up maneuver is well predicted, especially the large pressure variation on the leeward side, at locations $x \geq 0.44$ and pitch angles $\alpha \geq 15$ deg. The leeward side vortices induce strong and cohesive swirling motions on the body surface, which results in suction peaks in the leeward side at $x = 0.44$ and 0.77 and $\alpha = 20$–30 deg. Toward the trailing edge of the body, both the computational and experimental results show flattened C_p, which indicates detached vortices. As expected from the large errors in C_N prediction, however, suction

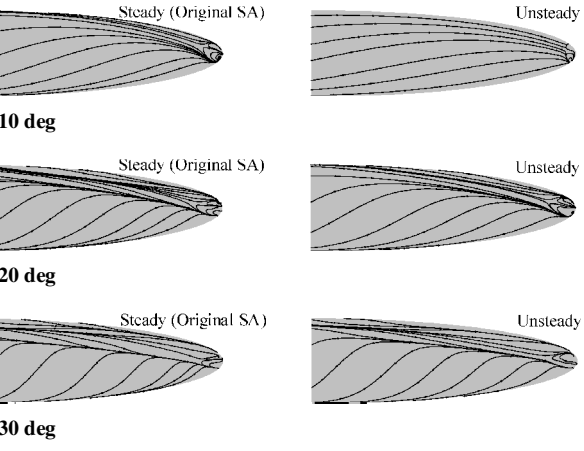

Fig. 8 Skin-friction lines on aftbody.

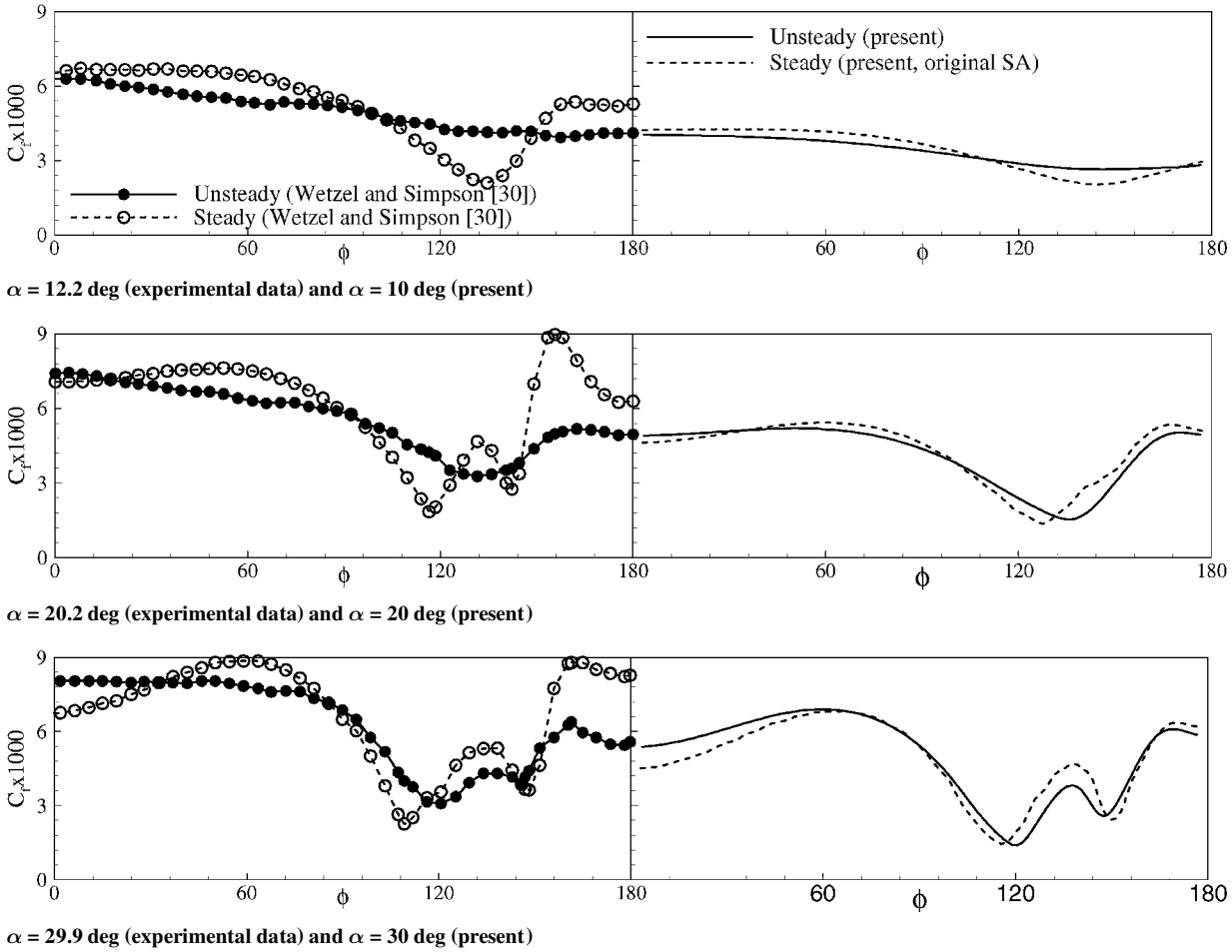

Fig. 9 Difference of skin-friction coefficient between steady and unsteady cases at $x = 0.729$.

peaks are underpredicted at higher pitch angle and near the trailing edge, which is related to the weaker vortices in the computational results shown earlier.

Skin-friction coefficient, $C_f = \tau_{\text{wall}}/\frac{1}{2}\rho U_0^2$, at various axial locations, $x = 0.118, 0.424, 0.729$, and 0.882, are presented in Fig. 7 for increasing pitch angles. Experimental data[‡] are also shown for comparison. The overall agreement is good and the trend of the computational results compare favorably with the experimental data, although the difference seems to be larger than that of C_p comparisons. The increasing difference with increasing x on the windward side at small pitch angles does not seem to be justifiable, and the authors suspect possible relaminarization of flow in the experiment, which cannot be simulated by the present method. C_f values at local minima are underpredicted, supporting the argument of overpredicted eddy viscosity. The good agreement in the locations of local minima indicate that the flow development patterns are well predicted, although the computational results show slightly slower separation formation, that is, approximately 5-deg leeward shift, as shown in Fig. 5.

The difference in the flow development patterns for the steady and the unsteady flow cases can be viewed in Fig. 8 by the skin-friction lines near the trailing edge at $\alpha = 10$, 20, and 30 deg. The unsteady flow results clearly display the delayed separations, and the milder crossflow reveals the history effect of particle movement in the unsteady flow. The difference is also shown in Fig. 9, which shows direct comparisons between steady and unsteady C_f at $x = 0.729$ for the same incidence angles. The present results correctly predict the trend in the difference, such that there is 1) clear separation (steady) and no separation (unsteady) at $\alpha = 10$ deg, 2) primary and secondary separation (steady) and leeward shifted primary separation only (unsteady) at $\alpha = 20$ deg, and 3) strong primary and secondary separation (steady) and leeward shifted primary separation and weak secondary separation (unsteady) at $\alpha = 30$ deg. This trend also confirms the argument that, in an unsteady flow, the separation pattern can be quite different from its counterpart in an equivalent steady configuration.

VI. Conclusions

A three-dimensional RANS method for unsteady turbulent flow around a maneuvering vehicle was developed and applied to a model problem concerning an extreme case of submarine maneuvers, that is, a 6:1 prolate spheroid is pitched about its center while advancing forward. A body force term is added in the RANS equations to take into account the inertial motion in the body-fixed coordinate system. The one-equation SA turbulence model is employed for turbulence closure.

An artificial compressibility is introduced into the continuity equation for velocity–pressure coupling. The governing equations are discretized by second-order accurate FVM in space and second-order-accurate backward scheme in time. Although the code is constructed for general unstructured cell grids, hexahedral cell grids are used in the present study to exploit the simplicity of the geometry.

The computational results are analyzed with global and local quantities and validated by comparison with experimental data. Overall, the present method performs quite well in predicting the unsteady flow phenomena around a maneuvering prolate spheroid and the results compare well with available experimental data. From the comparison of steady and unsteady flow results, it was found that there are lags in the flowfield development and delays of separation in unsteady flow cases, indicating that unsteady flow phenomena cannot be accurately captured by simple extensions of steady or quasi-steady computational results. Comparisons with experimental data reveal, however, that the isotropic eddy viscosity turbulence model employed for the present study does not adequately resolve the vortical flow in the leeward side of the body.

The results of the study suggest applicability of the present approach for additional complexities such as practical geometry with appendages, more realistic maneuvering motions, and maneuvering performance prediction of self-propelled vehicles. However, some improvements are warranted. In particular, more advanced turbulence models, such as the Reynolds stress model, might be needed to predict the secondary flow and streamwise vortices. Also, improvement of computational efficiency is recommended to enhance the usability of the code in practical design procedures.

Acknowledgment

The financial support for the first author from the Ministry of Education, Culture, Sport, Science and Technology of Japan, while he was a Science and Technology Agency Fellow, is gratefully acknowledged.

References

[1]Wetzel, T. G., and Simpson, R. L., "Unsteady Crossflow Separation Location Measurements on a Maneuvering 6:1 Prolate Spheroid," *AIAA Journal*, Vol. 36, No. 11, 1998, pp. 2063–2071.

[2]Taylor, L. K., Arabshahi, A., and Whitfield, D. L., "Unsteady Three-Dimensional Incompressible Navier–Stokes Computations for a Prolate Spheroid Undergoing Time-Dependent Maneuvers," AIAA Paper 95-0313, 1995.

[3]Han, T., and Patel, V. C., "Flow Separation on a Spheroid at Incidence," *Journal of Fluid Mechanics*, Vol. 92, Pt. 4, 1979, pp. 643–658.

[4]Costis, C. E., Hoang, N. T., and Telionis, D. P., "Laminar Separating Flow over a Prolate Spheroid," *Journal of Aircraft*, Vol. 26, No. 9, 1989, pp. 810–816.

[5]Tobak, M., and Peake, D. J., "Topology of Three-dimensional Separated Flows," *Annual Review of Fluid Mechanics*, Vol. 14, 1982, pp. 61–85.

[6]Wang, K. C., "Boundary Layer over a Blunt Body at Low Incidence with Circumferential Reversed Flow," *Journal of Fluid Mechanics*, Vol. 72, Pt. 1, 1975, pp. 49–65.

[7]Cebeci, T., and Su, W., "Separation of Three-Dimensional Laminar Boundary Layers on a Prolate Spheroid," *Journal of Fluid Mechanics*, Vol. 191, 1988, pp. 47–77.

[8]Yates, L. A., and Chapman, G. T., "Streamlines, Vorticity Lines, and Vortices Around Three-Dimensional Bodies," *AIAA Journal*, Vol. 30, No. 7, 1992, pp. 1819–1826.

[9]Meier, H. U., Kreplin, H. P., Landhaußer, A., and Baumgarten, D., "Mean Velocity Distributions in Three-dimensional Boundary Layers Developing on a 1:6 Prolate Spheroid with Natural Transition," DFVLR, Data Rept. DFVLR IB 222-4 A 10, Göttingen, Germany, 1984.

[10]Meier, H. U., Kreplin, H. P., and Landhaußer, A., "Wall Pressure Measurements on a 1:6 Prolate Spheroid in the DFVLR 3×3 m Low Speed Wind Tunnel ($\alpha = 10^\circ$, $U_\infty = 55$ m/s, Artificial Transition)," DFVLR, Data Rept. DFVLR IB 222-86 A 04, Göttingen, Germany, 1986.

[11]Barber, K. M., and Simpson, R. L., "Mean Velocity and Turbulence Measurements of Flow Around a 6:1 Prolate Spheroid," AIAA Paper 91-0255, 1991.

[12]Chesnakas, C. J., and Simpson, R. L., "Detailed Investigation of the Three-Dimensional Separation about a 6:1 Prolate Spheroid," *AIAA Journal*, Vol. 35, No. 6, 1997, pp. 990–999.

[13]Kreplin, H.-P., and Stäger, R., "Measurements of the Reynolds-Stress Tensor in the Three-dimensional Boundary Layer of an Inclined Body of Revolution," *Proceedings of the 9th Symposium on Turbulent Shear Flows*, Kyoto Univ., Kyoto, Japan, 1993, pp. 2-4-1–2-4-6.

[14]Barberis, D., and Molton, P., "Experimental Study of Three-Dimensional Separation on a Large-Scale Model," *AIAA Journal*, Vol. 33, No. 1, 1995, pp. 2107–2113.

[15]Kim, S. E., and Patel, V. C., "Separation on a Spheroid at Incidence: Turbulent Flow," *Proceeding of the 2nd Osaka Colloquium on Viscous Fluid Dynamics in Ship and Ocean Technology*, Osaka Univ. and Univ. of Osaka Prefecture, Osaka, Japan, 1991, pp. 29–55.

[16]Gee, K., Cummings, R. M., and Schiff, L. B., "Turbulence Model Effects on Separated Flow About a Prolate Spheroid," *AIAA Journal*, Vol. 30, No. 2, 1992, pp. 655–664.

[17]Piquet, J., and Queutey, P., "Navier–Stokes Computations Past a Prolate Spheroid at Incidence—I. Low Incidence Case," *Computers and Fluids*, Vol. 21, No. 4, 1992, pp. 599–625.

[18]Piquet, J., and Queutey, P., "Navier–Stokes Computations Past a Prolate Spheroid at Incidence—II. High Incidence Case," *International Journal for Numerical Methods in Fluids*, Vol. 16, No. 1, 1993, pp. 1–27.

[19]Sung, C.-H., Griffin, M. J., Tsai, J. F., and Huang, T. T., "Incompressible Flow Computation of Forces and Moments on Bodies of Revolution at Incidence," AIAA Paper 93-0787, 1993.

[20]Sung, C.-H., Fu, T. C., Griffin, M. J., and Huang, T. T., "Validation of Incompressible Flow Computation of Forces and Moments on Axisymmetric Bodies at Incidence," AIAA Paper 95-0528, 1995.

[21]Sturek, W. B., Birch, T., Lauzon, M., Housch, C., Manter, J., Josyula, E., and Soni, B., "The Application of CFD to the Prediction of Missile Body Vortices," AIAA Paper 97-0637, 1997.

[22]Rhee, S. H., and Hino, T., "Computational Investigation of 3D Turbulent Flow Separation around a Spheroid using an Unstructured Grid Method," *Journal of Society of Naval Architects of Japan*, Vol. 188, Dec. 2000, pp. 1–9.

[23]Smith, L. H., and Nunn, R. H., "Aerodynamic Characteristics of an Axisymmetric Body Undergoing a Uniform Pitching Motion," *Journal of Spacecraft and Rockets*, Vol. 13, No. 1, 1976, pp. 8–14.

[24]Gad-el-Hak, M., and Ho, C.-M., "Unsteady Flow Around an Ogive Cylinder," *Journal of Aircraft*, Vol. 23, No. 6, 1986, pp. 520–528.

[25]Montividas, R., Reisenthel, P., and Nagib, H., "Scaling and Control of Vortex Geometry Behind Pitching Cylinders," AIAA Paper 89-1003, 1989.

[26]Panzer, E. C., Rediniotis, P. K., and Telionis, D. P., "The Hemisphere-Cylinder in Dynamic Pitch-Up Motions," AIAA Paper 93-2963, 1993.

[27]Rediniotis, O. K., Hoang, N. T., and Telionis, D. P., "Hemisphere-Cylinder in Dynamic Pitch-Up Motions," *AIAA Journal*, Vol. 37, No. 12, 1999, pp. 1673–1675.

[28]Hoang, N. T., Wetzel, T. G., and Simpson, R. L., "Unsteady Measurements over a 6:1 Prolate Spheroid Undergoing a Pitch-Up Maneuver," AIAA Paper 94-0197, 1994.

[29]Hoang, N. T., Wetzel, T. G., and Simpson, R. L., "Surface Pressure Measurements over a 6:1 Prolate Spheroid Undergoing Time-Dependent Maneuvers," AIAA Paper 94-1908-CP, 1994.

[30]Wetzel, T. G., and Simpson, R. L., "Unsteady Three-Dimensional Cross-flow Separation Measurements on a Prolate Spheroid Undergoing Time-Dependent Maneuvers," AIAA Paper 97-0618, 1997.

[31]Sung, C.-H., Fu, T. C., Griffin, M. J., and Huang, T. T., "Validation of Incompressible Flow Computation of Forces and Moments on Axisymmetric Bodies Undergoing Constant Radius Turning," *Proceedings of the 21st Symposium on Naval Hydrodynamics*, National Academy Press, Trondheim, Norway, 1996, pp. 1048–1060.

[32]Sato, T., Izumi, K., and Miyata, H., "Numerical Simulation of Maneuvering Motion," *Proceedings of the 22nd Symposium on Naval Hydrodynamics*, National Academy Press, Washington, DC, 1998, pp. 724–735.

[33]Stanek, M. J., and Visbal, M. R., "Investigation of Vortex Development on a Pitching Slender Body of Revolution," AIAA Paper 91-3273, 1991.

[34]McDonald, H., and Whitfield, D., "Self-propelled Maneuvering Underwater Vehicles," *Proceedings of the 21st Symposium on Naval Hydrodynamics*, National Academy Press, Trondheim, Norway, 1996, pp. 478–489.

[35]Spalart, P. R., and Allmaras, S. R., "A One-Equation Turbulence Model for Aerodynamic Flows," AIAA Paper 92-0439, 1992.

[36]Dacles-Mariani, J., Zilliac, G. G., Chow, J. S., and Bradshaw, P., "Numerical/Experimental Study of a Wingtip Vortex in the Near Field," *AIAA Journal*, Vol. 33, No. 9, 1995, pp. 1561–1568.

[37]Hino, T., "A 3D Unstructured Grid Method for Incompressible Viscous Flows," *Journal of Society of Naval Architects of Japan*, Vol. 182, Dec. 1997, pp. 9–15.

[38]Hino, T., "An Interface Capturing Method for Free Surface Flow Computations on Unstructured Grids," *Journal of Society of Naval Architects of Japan*, Vol. 186, Dec. 1999, pp. 177–183.

[39]Rhee, S. H., and Hino, T., "Unstructured Grid Flow Solver for Practical Ship Hulls," *Proceedings of Gothenburg 2000—A Workshop on Numerical Ship Hydrodynamics*, Chalmers Univ., Gothenburg, Sweden, 2000.

[40]Rogers, S. E., Kwak, D., and Kiris, C., "Steady and Unsteady Solutions of the Incompressible Navier–Stokes Equations," *AIAA Journal*, Vol. 29, No. 4, 1991, pp. 603–610.

[41]Rhee, S. H., and Hino, T., "Unstructured Grid Flow Solver for Ship Flows," *Proceedings of the 4th International Conference on Hydrodynamics*, Ship and Ocean Foundation, Yokohama, Japan, 2000, pp. 243–248.

[42]Roe, P. L., "Characteristic-Based Schemes for the Euler Equations," *Annual Review of Fluid Mechanics*, Vol. 18, 1986, pp. 337–365.

[43]Roache, P. J., *Verification and Validation in Computational Science and Engineering*, *Part II. Verification*, Hermosa, Albuquerque, NM, 1998.

R. M. C. So
Associate Editor